Journal of Medicinal Chemistry

- Supporting Information
- Access to high resolution figures
- Links to articles and content related to this article
- Copyright permission to reproduce figures and/or text from this article

View the Full Text HTML

Improving Tumor Uptake and Excretion Kinetics of ^{99m}Tc-Labeled Cyclic Arginine-Glycine-Aspartic (RGD) Dimers with Triglycine Linkers

Jiyun Shi,[†] Lijun Wang,[†] Young-Seung Kim,[†] Shizhen Zhai,[†] Zhaofei Liu,[‡] Xiaoyuan Chen,[‡] and Shuang Liu*,[†]

School of Health Sciences, Purdue University, 550 Stadium Mall Drive, Indiana 47907, Molecular Imaging Program at Stanford, Department of Radiology & Bio-X, Stanford University, Stanford, California

This report describes the synthesis of two new cyclic RGD (Arg-Gly-Asp) dimers, **3** (E[G$_3$-c(RGDfK)]$_2$) and **4** (G$_3$-E[G$_3$-c(RGDfK)]$_2$), and their corresponding conjugates **5** (HYNIC-E[G$_3$-c(RGDfK)]$_2$: HYNIC = 6-(2-(2-sulfonatobenzaldehyde)hydrazono)nicotinyl) and **6** (HYNIC-G$_3$-E[G$_3$-c(RGDfK)]$_2$). Integrin $\alpha_v\beta_3$ binding affinities of **5** and **6** were determined by displacement of ^{125}I-echistatin bound to U87MG glioma cells. ^{99m}Tc complexes **7** ([^{99m}Tc(**5**)(tricine)(TPPTS)]: TPPTS = trisodium triphenylphosphine-3,3′,3″-trisulfonate) and **8** ([^{99m}Tc(**6**)(tricine)(TPPTS)]) were prepared in high yield and high specific activity. Biodistribution and imaging studies were performed in athymic nude mice bearing U87MG glioma and MDA-MB-435 breast cancer xenografts. It was found that G$_3$ linkers are particularly useful for increasing integrin $\alpha_v\beta_3$ binding affinity of cyclic RGD dimers and improving the tumor uptake and clearance kinetic of their ^{99m}Tc radiotracers. Complex **8** is a very promising radiotracer for the early detection of integrin $\alpha_v\beta_3$-positive tumors and may have the potential for noninvasive monitoring of tumor growth or shrinkage during antiangiogenic treatment.

Introduction

Angiogenesis is a requirement for tumor growth and metastasis.[1−10] Without the neovasculature to provide oxygen and nutrients, tumors cannot grow beyond 1−2 mm in size. Once vascularized, previously dormant tumors begin to grow rapidly and their volumes increase exponentially. The angiogenic process depends on vascular endothelial cell migration and invasion and is regulated by cell adhesion receptors. Integrins are a family of proteins that facilitate cellular adhesion to and migration on extracellular matrix proteins found in intercellular spaces and basement membranes and regulate cellular entry and withdraw from the tumor cell cycle.[4−13] Integrin $\alpha_v\beta_3$ is a receptor for extracellular matrix proteins with the exposed arginine-glycine-aspartic (RGD[a]) tripeptide sequence.[5,6,9] Integrin $\alpha_v\beta_3$ is normally expressed at low levels on epithelial cells and mature endothelial cells, but it is highly expressed on the neovasculature of tumors, including osteosarcomas, glioblas-

tomas, melanomas, lung carcinomas, and breast cancer.[13−19] It has been demonstrated that integrin $\alpha_v\beta_3$ is overexpressed on both endothelial and tumor cells in human breast cancer xenografts,[20] and the integrin $\alpha_v\beta_3$ expression correlates well with tumor progression and invasiveness of melanoma, glioma, and breast cancers.[13−20] The highly restricted expression of integrin $\alpha_v\beta_3$ during tumor growth, invasion, and metastasis presents an interesting molecular target for early detection of rapidly growing and metastatic tumors.[21−33] In addition, it would be highly advantageous to develop an integrin $\alpha_v\beta_3$-specific radiotracer that could be used to noninvasively visualize and quantify the integrin $\alpha_v\beta_3$ expression level before, during, and/or after antiangiogenic therapy.

Over the past decade, many radiolabeled cyclic RGD peptides were evaluated as new integrin $\alpha_v\beta_3$-targeted radiotracers for imaging tumors by positron emission tomography (PET) or single photon emission computed tomography (SPECT).[34−68] They have been reviewed extensively.[21−33] Among the radiotracers evaluated in different preclinical tumor-bearing animal models, [^{18}F]-AH111585, the core peptide sequence originally discovered from a phage display library (such as ACDRGD-CFCG),[69] and [^{18}F]galacto-RGD (2-[^{18}F]fluoropropanamide c(RGDfK(SAA); SAA = 7-amino-L-glyero-L-galacto-2,6-anhydro-7-deoxyheptanamide) are under clinical investigations for noninvasive visualization of integrin $\alpha_v\beta_3$ expression in cancer patients.[69−71] The imaging studies in cancer patients show that the ^{18}F-labeled cyclic RGD peptides are able to target the integrin $\alpha_v\beta_3$-positive tumors. However, the low tumor uptake, high cost, and lack of preparation modules for the ^{18}F-labeled monomeric cyclic RGD peptides impose significant challenges to their continued clinical applications. To improve integrin $\alpha_v\beta_3$ binding affinity, we and others have been using multimeric cyclic RGD peptides, such as E[c(RGDfK)]$_2$ (**1**) and E{E[c(RGDfK)]$_2$}$_2$ (**2**), to develop integrin $\alpha_v\beta_3$-targeted radiotracers.[47−68] It was found that multimerization of cyclic RGD peptides enhances their integrin $\alpha_v\beta_3$ binding affinity and improves the radiotracer tumor uptake. However, the kidney

* To whom correspondence should be addressed. Phone: 765-494-0236. Fax 765-496-1377. E-mail: lius@pharmacy.purdue.edu.
† School of Health Sciences, Purdue University.
‡ Molecular Imaging Program at Stanford, Department of Radiology & Bio-X, Stanford University.

^{a} Abbreviations: E[c(RGDfK)]$_2$, Glu[cyclo(Lys-Arg-Gly-Asp-D-Phe)-cyclo(Lys-Arg-Gly-Asp-D-Phe)]; E[G$_3$-c(RGDfK)]$_2$, Glu{cyclo[Lys-Gly-Gly-Gly)-Arg-Gly-Asp-D-Phe]-cyclo[Lys(Gly-Gly-Gly)-Arg-Gly-Asp-D-Phe]}; G$_3$-E[G$_3$-c(RGDfK)]$_2$, (Gly-Gly-Gly)-Glu{cyclo[Lys-Gly-Gly-Gly)-Arg-Gly-Asp-D-Phe]-cyclo[Lys(Gly-Gly-Gly)-Arg-Gly-Asp-D-Phe]}; E{E[c(RGDfK)]$_2$}$_2$, Glu{Glu[cyclo(Lys-Arg-Gly-Asp-D-Phe)]-cyclo(Lys-Arg-Gly-Asp-D-Phe)}-{Glu[cyclo(Lys-Arg-Gly-Asp-D-Phe)]-cyclo(Lys-Arg-Gly-Asp-D-Phe)}; HYNIC, 6-(2-(2-sulfonatobenzaldehyde)hydrazono)nicotinyl; HYNIC-E[c(RGDfK)]$_2$, 6-(2-(2-sulfonatobenzaldehyde)hydrazono)nicotinyl-Glu[cyclo(Lys-Arg-Gly-Asp-D-Phe)-cyclo(Lys-Arg-Gly-Asp-D-Phe)]; HYNIC-E[G$_3$-c(RGDfK)]$_2$, 6-(2-(2-sulfonatobenzaldehyde)hydrazono)nicotinyl-Glu{cyclo[Lys(Gly-Gly-Gly)-Arg-Gly-Asp-D-Phe]-cyclo[Lys(Gly-Gly-Gly)-Arg-Gly-Asp-D-Phe]}; HYNIC-G$_3$-E[G$_3$-c(RGDfK)]$_2$, 6-(2-(2-sulfonatobenzaldehyde)hydrazono)nicotinyl-(Gly-Gly-Gly)-Glu{cyclo[Lys(Gly-Gly-Gly)-Arg-Gly-Asp-D-Phe]-cyclo[Lys(Gly-Gly-Gly)-Arg-Gly-Asp-D-Phe]}; HYNIC-E{E[c(RGDfK)]$_2$}$_2$, 6-(2-(2-sulfonatobenzaldehyde)hydrazono)nicotinyl-Glu{Glu[cyclo(Lys-Arg-Gly-Asp-D-Phe)]-cyclo(Lys-Arg-Gly-Asp-D-Phe)}-{Glu[cyclo(Lys-Arg-Gly-Asp-D-Phe)]-cyclo(Lys-Arg-Gly-Asp-D-Phe)}; TPPTS, trisodium triphenylphosphine-3,3′,3″-trisulfonate.
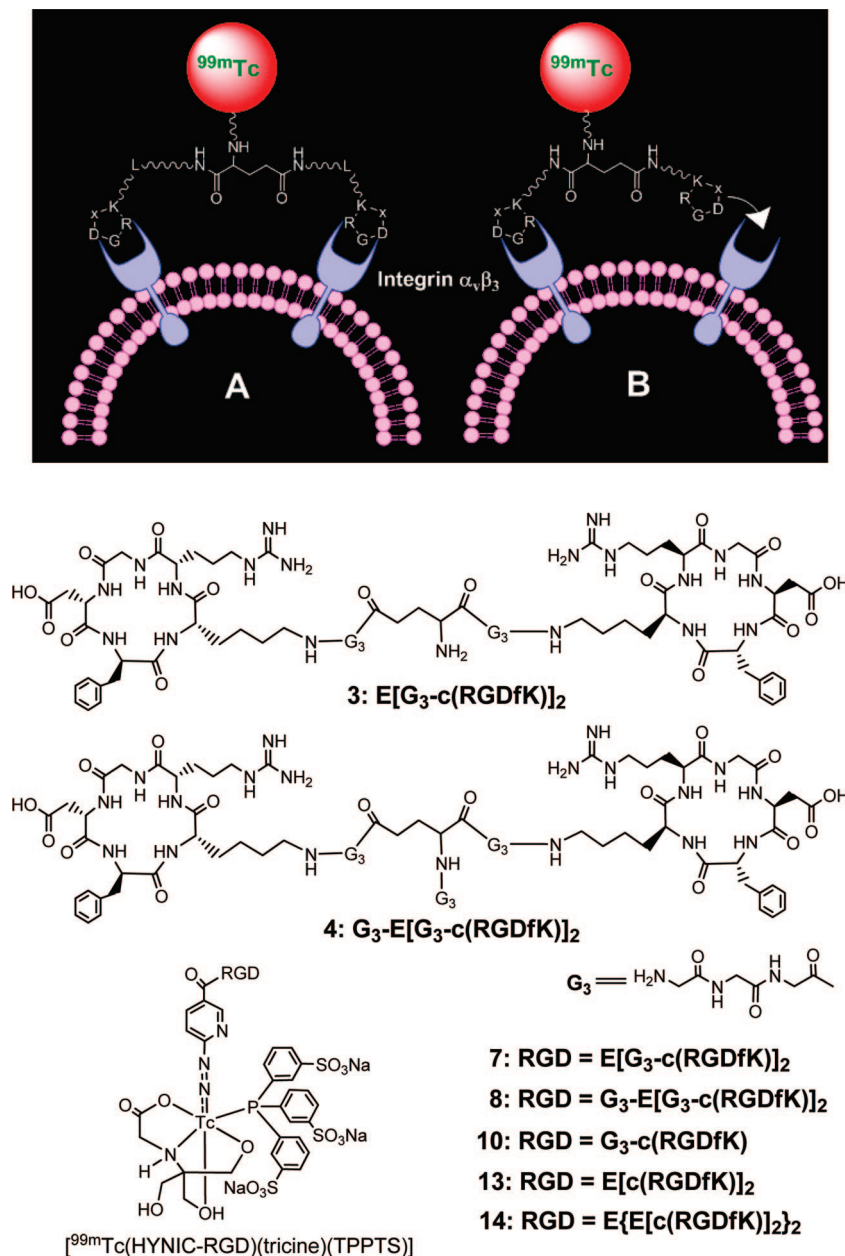
Figure 1. Top: the schematic illustration of interactions between cyclic RGD peptide dimers and integrin $\alpha_v\beta_3$. (A) The distance between two RGD motifs is long due to the presence of two linkers (L). As a result, the cyclic RGD dimer is able to bind integrin $\alpha_v\beta_3$ in a "bivalent" fashion. (B) The distance between two RGD motifs is not long enough for simultaneous integrin $\alpha_v\beta_3$ binding. However, the RGD concentration is "locally enriched" in the vicinity of neighboring integrin $\alpha_v\beta_3$ once the first RGD motif is bound. In both cases, the end-result would be higher integrin $\alpha_v\beta_3$ binding affinity for the multimeric cyclic RGD peptides. Bottom: cyclic RGD dimers (**3** and **4**), their 99mTc complexes, [99mTc(**5**)(tricine)(TPPTS)] (**7**), and [99mTc(**6**)(tricine)(TPPTS)] (**8**) to be evaluated in this study.

and liver uptake of radiolabeled cyclic RGD peptides was also increased significantly as the peptide multiplicity increases.[47,57-61]

To solve the problem, we prepared two novel cyclic RGD peptide dimers, **3** (Figure 1: E[G$_3$-c(RGDfK)]$_2$) and **4** (Figure 1: G$_3$-E[G$_3$-c(RGDfK)]$_2$), and their HYNIC (6-(2-(2-sulfonato-benzaldehyde)hydrazono)nicotinyl) conjugates, **5** (HYNIC-E[G$_3$-c(RGDfK)]$_2$ and **6** (HYNIC-G$_3$-E[G$_3$-c(RGDfK)]$_2$). The triglycine (G$_3$) linkers were used for two main purposes: (1) to increase the distance between two cyclic RGD motifs from 6 bonds in **1** to 26 bonds in **3** and **4** (excluding side arms of K-residues) so that they can achieve simultaneous integrin $\alpha_v\beta_3$ binding and (2) to improve radiotracer excretion kinetics from noncancerous organs, such as kidneys, liver, and lungs. We are particularly interested in 99mTc due to its optimal nuclear properties, easy availability, and low cost.[72-74] For 99mTc-

labeling, HYNIC was used as a bifunctional coupling agent, while tricine and TPPTS (trisodium triphenylphosphine-3,3′,3″-trisulfonate) were used as coligands to prepare 99mTc complexes **7** (Figure 1: [99mTc(**5**)(tricine)(TPPTS)]) and **8** (Figure 1: [99mTc(**6**)(tricine)(TPPTS)]). The integrin $\alpha_v\beta_3$ binding affinity of **5** and **6** was determined by competitive replacement of 125I-echistatin bound to U87MG human glioma cells. Biodistribution properties of **7** and **8** were evaluated in the athymic nude mice bearing U87MG human glioma and MDA-MB-435 breast cancer xenografts. For comparison purposes, we also evaluated cyclic RGD monomer conjugate **9** (HYNIC-G$_3$-c(RGDfK)) and its ternary ligand 99mTc complex **10** ([99mTc(**9**)(tricine)(TPPTS)]) using the same in vitro and in vivo assays. Imaging studies were performed to evaluate **7** and **8** as new SPECT radiotracers for imaging integrin $\alpha_v\beta_3$-positive tumors. The main objective of

this study is to demonstrate that G_3 linkers are useful for enhancing integrin $\alpha_v\beta_3$ binding affinity of cyclic RGD peptide dimers and improving the tumor uptake and excretion kinetics of their ^{99m}Tc radiotracers from noncancerous organs. Improvement of radiotracer tumor uptake and excretion kinetics from kidneys, liver, and lungs is critically important for early detection of the integrin $\alpha_v\beta_3$-positive tumors.

Experimental Section

Materials and Methods. Chemicals were purchased from Sigma-Aldrich (St. Louis, MO) and were used without further purification. Cyclic RGD peptides, E[G_3-c(RGDfK)]$_2$, G_3-E[G_3-c(RGDfK)]$_2$, and G_3-c(RGDfK) were custom-made by the Peptides International, Inc. (Louisville, KY). Sodium succinimidyl 6-(2-(2-sulfonatobenzaldehyde)hydrazono)nicotinate (HYNIC-NHS) was prepared according to literature method.[75] Na^{99m}TcO$_4$ was obtained from a commercial DuPont Pharma ^{99}Mo/^{99m}Tc generator (N. Billerica, MA). The ESI (electrospray ionization) mass spectral data were collected on a Finnigan LCQ classic mass spectrometer, School of Pharmacy, Purdue University. HPLC method 1 used a LabAlliance HPLC system equipped with a UV/vis detector ($\lambda = 254$ nm) and Zorbax C$_{18}$ semiprep column (9.4 mm × 250 mm, 100 Å pore size). The flow rate was 2.5 mL/min. The gradient mobile phase started with 95% solvent A (0.1% TFA in H$_2$O) and 5% solvent B (0.1% TFA in CH$_3$CN) to 60% solvent A and 40% solvent B at 25 min to 40% solvent A and 60% solvent B at 30 min. The radio-HPLC method (method 2) used the LabAlliance HPLC system (State College, PA) equipped with a β-ram IN/US detector (IN/US System, Tampa, FL) and Zorbax C$_{18}$ column (4.6 mm × 250 mm, 300 Å pore size; Agilent Technologies, Santa Clara, CA). The flow rate was 1 mL/min. The mobile phase was isocratic with 90% solvent A (25 mM NH$_4$OAc buffer, pH = 5.0) and 10% solvent B (CH$_3$CN) at 0 − 2 min, followed by a gradient mobile phase going from 10% solvent B at 2 min to 15% solvent B at 5 min, and 20% solvent B at 20 min.

Conjugate 5. HYNIC-NHS (10.2 mg, 24.4 μmol) and **3** (6.3 mg, 3.8 μmol) were dissolved in DMF (2 mL). After addition of triethylamine (10 mg, 10 μmol), the reaction mixture was stirred at room temperature overnight. The product was isolated from the reaction mixture by HPLC purification (method 1). The fraction at 18.5 min was collected. Lyophilization of the collected fractions afforded **5** as a white powder. The yield was 4.0 mg (~54%) with >95% HPLC purity. ESI-MS (positive mode): $m/z = 1964.43$ for [M + H]$^+$ (1962.80 calcd for [C$_{84}$H$_{114}$N$_{28}$O$_{26}$S]$^+$).

Conjugate 6. HYNIC-NHS (8.7 mg, 20.9 μmol) and **4** (8.1 mg, 4.4 μmol) were dissolved in anhydrous DMF (2 mL). After addition of triethylamine (10 mg, 10 μmol), the reaction mixture was stirred at room temperature overnight. The product was isolated by HPLC purification (method 1). Fractions at 18.1 min were collected. Lyophilization of the combined collections afforded **6**. The yield was 5.6 mg (~60%) with >95% HPLC purity. ESI-MS: $m/z = 2136.60$ for [M + H]$^+$ (2134.89 calcd For [C$_{90}$H$_{123}$N$_{31}$O$_{29}$S]$^+$).

Conjugate 9. It was prepared according to the same procedure above using HYNIC-NHS (10.8 mg, 25.8 μmol) and G_3-c(RGDfK) (5 mg, 6.45 μmol). Lyophilization of the collected fractions ~16.8 min (method 1) afforded the expected conjugate **9**. The yield was 3.1 mg (~45%) with HPLC purity >95%. ESI-MS: $m/z = 1078.29$ for [M + H]$^+$ (1077.41 calcd For [C$_{46}$H$_{59}$N$_{15}$O$_{14}$S]$^+$)

^{99m}Tc-Labeling and Dose Preparation. To a lyophilized vial containing 5 mg of TPPTS, 6.5 mg of tricine, 38.5 mg of disodium succinate hexahydrate, and 12.7 mg of succinic acid, 20 μg of the cyclic RGD peptide conjugate (**5**, **6** and **9**) was added 1.0−1.5 mL of Na[^{99m}TcO$_4$] solution (10 − 50 mCi) in saline. The vial was heated at 100 °C for 10−15 min in a lead-shielded water bath. After heating, the vial was placed back into the lead pig, and allowed to stand at room temperature for ~10 min. A sample of the resulting solution was analyzed by the radio-HPLC (method 2) and ITLC. For biodistribution studies, all radiotracers were purified by HPLC (method 2). Volatiles in the HPLC mobile phase were removed under vacuum. Doses were prepared by dissolving the purified radiotracer in saline to 20−30 μCi/mL. For imaging studies, doses were prepared by dissolving the radiotracer in saline to ~5 mCi/mL. For the blocking experiment, **1** was dissolved in the solution containing the radiotracer to give a concentration of 3.5 mg/mL. The resulting solution was filtered with a 0.20 μm Millex-LG filter unit before being injected into animals. Each tumor-bearing mouse was injected with 0.1−0.2 mL of the dose solution.

Partition Coefficient Determination. The radiotracer was purified by HPLC (method 2). Volatiles were removed completely under vacuum. The residue was dissolved in a equal volume (3 mL:3 mL) mixture of n-octanol and 25 mM phosphate buffer (pH = 7.4). After stirring for ~20 min, the mixture was centrifuged at 8000 rpm for 5 min. Samples (in triplets) from n-octanol and aqueous layers were counted in a Perkin-Elmer Wizard-1480 γ-counter (Shelton, CT). The log P value was reported as an average of three independent measurements plus the standard deviation.

In Vitro Whole-Cell Integrin $\alpha_v\beta_3$ Binding Assay. The in vitro integrin binding affinity and specificity of RGD peptides were assessed via a cellular competitive displacement assay using ^{125}I-echistatin as the integrin-specific radioligand.[50,52] Briefly, U87MG human glioma cells were grown in Gibco's Dulbecco's medium supplemented with 10% fetal bovine serum (FBS), 100 IU/mL penicillin and 100 μg/mL streptomycin (Invitrogen Co, Carlsbad, CA), at 37 °C in humidified atmosphere containing 5% CO$_2$. Filter multiscreen DV plates were seeded with 10^5 glioma cells in binding buffer and incubated with ^{125}I-echistatin in the presence of increasing concentrations of different cyclic RGD peptides. After removing the unbound ^{125}I-echistatin, hydrophilic PVDF filters were collected and the radioactivity was determined using a gamma counter (Packard, Meriden, CT). The IC$_{50}$ values were calculated by fitting the experimental data with the nonlinear regression using GraphPad Prism (GraphPad Software, Inc., San Diego, CA). Experiments were carried out twice with triplicate samples. The IC$_{50}$ values are reported as an average of these samples plus the standard deviation.

Animal Model. Biodistribution and imaging studies were performed using the athymic nude mice bearing U87MG human glioma and MDA-MB-435 human breast cancer xenografts in compliance NIH animal experiment guidelines (*Principles of Laboratory Animal Care*, NIH Publication no. 86-23, revised 1985). The animal protocol for these studies has been approved by the Purdue University Animal Care and Use Committee (PACUC). U87MG glioma and MDA-MB-435 breast cancer cells were grown at 37 °C in Minimal Essential Medium (Alpha Modification) containing 3.7 g of sodium bicarbonate/L, 10% fetal bovine serum v/v, in a humidified atmosphere of 5% carbon dioxide. Female athymic nu/nu mice were purchased from Harlan (Indianapolis, IN) at 4−5 weeks of age. Each mouse was implanted subcutaneously with 5 × 10^6 tumor cells into the left and right upper flanks for the glioma model, or into the left and right mammary fat pads for the breast cancer model. In this way, one could access the impact of tumor size on the radiotracer imaging quality in a single tumor-bearing mouse. Two to four weeks after inoculation, animals with tumors in the range of 0.1−1.0 g were used for biodistribution and imaging studies.

Biodistribution Protocol. Twelve tumor-bearing mice with the tumor size of 0.05−0.4 g were randomly divided into three groups. The ^{99m}Tc radiotracer (~2 μCi) in 0.1 mL saline was administered via tail vein. Once the animal was in surgical plane of anesthesia, the radiotracer (~2 μCi) in 0.1 mL saline was administered via tail vein. Four animals were sacrificed by sodium pentobarbital overdose (100 mg/kg) at 30, 60, and 120 min postinjection (pi). Blood samples were withdrawn from the heart. The tumor and normal organs (brain, eyes, spleen, lungs, liver, kidneys, muscle, and intestine) were excised, washed with saline, dried with absorbent tissue, weighed, and counted on a Perkin-Elmer Wizard-1480 γ-counter (Shelton, CT). The organ uptake was calculated as a percentage of the injected dose per organ (%ID/organ) and a percentage of the injected dose per gram of organ tissue (%ID/g). For the blocking experiment, four tumor-bearing nude mice (20−25 g) were used, and each animal was administered with ~2 μCi of **7**

along with ∼350 μg (∼14 mg/kg) of **1**. At 1 h pi, all four animals were sacrificed for organ biodistribution. The biodistribution data and target-to-background (T/B) ratios are reported as an average from four tumor-bearing mice at each time point plus the standard variation. Comparison between two different radiotracers was made using the two-way ANOVA test (GraphPad Prim 5.0, San Diego, CA). The level of significance was set at $p < 0.05$.

Scintigraphic Imaging. The athymic nude mice bearing the U87MG glioma or MDA-MB-435 breast cancer xenografts were used for scintigraphic imaging studies. Animals were anesthetized with intraperitoneal injection of sodium pentobarbital (45.0 mg/kg). Each animal was administered with 500−800 μCi of the radiotracer in 0.2 mL saline. Animals were placed prone on a single head mini γ-camera (Diagnostic Services Inc., NJ) equipped with a parallel-hole, low-energy, and high-resolution collimator. Static images were acquired at 15, 30, 60, and 120 min pi and were stored digitally in a 128 × 128 matrix. The acquisition count limits were set at 500 K. After completion of the imaging study, the tumor-bearing mice were euthanized by sodium pentobarbital overdose (100−200 mg/kg).

Metabolism. Normal athymic nude mice were used for metabolism studies. Each mouse was administered with the [99mTc] radiotracer (100−120 μCi). The urine samples were collected at 30 and 120 min pi by manual void and were mixed with equal volume of 20% acetonitrile aqueous solution. The mixture was centrifuged at 8000 rpm. The supernatant was collected and filtered through a 0.20 μm Millex-LG syringe-driven filter unit to remove any precipitate or particles. The filtrate was then analyzed by radio-HPLC (method 2). Tfhe feces samples were collected at 120 min pi and suspended in a mixture of 20% acetonitrile aqueous solution (2 mL). The resulting mixture was vortexed for 10 min. After centrifuging at 8000 rpm for 5 min, the supernatant was collected and passed through a 0.20 μm Millex-LG filter unit to remove any precipitate or particles. The filtrate was analyzed by radio-HPLC (method 2).

Results

Synthesis of Cyclic RGD Dimer Conjugates. Conjugates **5**, **6**, and **9** were prepared by direct conjugation of **3**, **4**, and G_3-c(RGDfK), respectively, with excess HYNIC-NHS in DMF. All new conjugates were purified by HPLC (method 1) and characterized by ESI-MS. The ESI-MS data were completely consistent with their proposed formula. Their HPLC purity of cyclic RGD dimer conjugates was >95% before being used for [99mTc]-labeling and determination of integrin $\alpha_v\beta_3$ binding affinity.

Integrin $\alpha_v\beta_3$ Binding Affinity. The integrin $\alpha_v\beta_3$ binding affinities of **5**, **6**, and **9** were determined by competitive displacement of [125I]-echistatin on the integrin $\alpha_v\beta_3$-positive U87MG glioma cells (Figure 2). For comparison purposes, we also evaluated **11** (HYNIC-E[c(RGDfK)]$_2$) and **12** (HYNIC-E{E[c(RGDfK)]$_2$}$_2$) using the same assay. IC$_{50}$ values for **9**, **11**, **5**, **6**, and **12** were calculated to be 357.5 ± 8.3, 112.2 ± 20.8, 60.3 ± 4.4, 61.1 ± 2.1, and 7.2 ± 1.5 nM, respectively.

Radiochemistry. Complexes **7**, **8**, and **10** were prepared according to the literature methods.[56,57] Their radiochemical purity (RCP) was >95% using the non-SnCl$_2$ formulation.[76] The specific activity was >10 Ci/μmol for all three radiotracers. They were analyzed by the reversed-phase HPLC method, and their HPLC retention times were 4.7, 9.2, and 10.5 min, respectively. All three new radiotracers were stable in the kit matrix for >12 h. It is interesting to note that complexes **7**, **8**, and **10** all showed a single radiometric peak in their radio-HPLC chromatograms. Because the Tc chelate is chiral, complexes [[99mTc](HYNIC-BM)(tricine)(TPPTS)] (BM = biomolecule) are often formed as a 50%:50% mixture of two diastereomers if the BM moiety contains one or more chiral centers.[74,77] Attempts
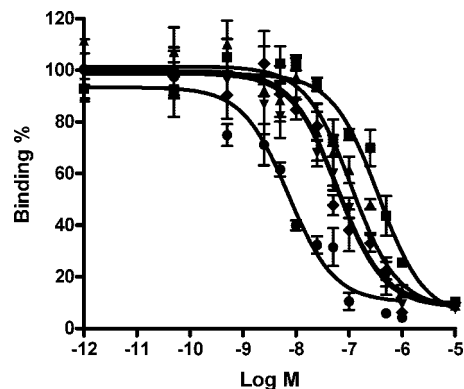

Figure 2. In vitro competitive inhibition curves of [125I]-echistatin bound to the integrin $\alpha_v\beta_3$-positive U87MG human glioma cells by **9** (□), **11** (▲), **5** (▼),**6** (◆), and **12** (●). Their IC$_{50}$ values were calculated to be 357.5 ± 8.3, 112.2 ± 20.8, 60.3 ± 4.4, 61.1 ± 2.1, and 7.2 ± 1.5 nM, respectively.

to separate the two diastereomers in **7**, **8**, and **10** were not successful using the chromatographic conditions described in this study. Apparently, the presence of G_3 groups makes separation of two diastereomers more difficult. We also determined the partition coefficients of **7**, **8**, and **10** in an equal volume mixture (3 mL:3 mL) of n-octanol and 25 mM phosphate buffer (pH = 7.4). Their log P values were calculated to be −4.30 ± 0.03, −4.44 ± 0.05, and −4.40 ± 0.19, respectively.

Biodistribution Characteristics in Breast Cancer Model. The athymic nude mice bearing MDA-MB-435 human breast cancer xenografts were used to evaluate the biodistribution characteristics and excretion kinetics of **7** and **8**. Figure 3 compares the tumor uptake and selected T/B ratios of complexes **7**, **8**, **13** ([[99mTc](**11**)(tricine)(TPPTS)]), and **14** ([[99mTc](**12**)-(tricine)(TPPTS)]). The biodistribution data for **7** and **8** are listed in Tables SI and SII of the Supporting Information, and those for **13** and **14** in the same tumor-bearing animal model were obtained from our previous reports.[32,58]

Complex **7** had the tumor uptake of 8.48 ± 0.59%ID/g at 30 min pi and 9.11 ± 1.83%ID/g at 120 min pi with very fast blood clearance (1.13 ± 0.21%ID/g and 0.30 ± 0.06%ID/g at 30 and 120 min pi, respectively). Its liver uptake was 4.20 ± 0.42%ID/g at 30 min pi and 2.68 ± 0.46%ID/g at 120 min pi. As a result, the tumor/liver ratios increased steadily over the 2 h study period (1.56 ± 0.37 at 30 min pi and 3.09 ± 0.76 at 120 min pi). The kidney uptake of **7** was 20.90 ± 3.49%ID/g and 10.74 ± 2.43% ID/g at 30 and 120 min pi, respectively. Its muscle uptake was 3.13 ± 1.04%ID/g at 30 min pi and 1.60 ± 0.32%ID/g at 120 min pi. The tumor/muscle ratio for **7** was 2.84 ± 0.93 at 30 min pi and 5.57 ± 0.69 at 120 min pi.

Complex **8** also had a high tumor uptake (8.34 ± 0.39%ID/g, 7.85 ± 0.94%ID/g, and 7.60 ± 0.68%ID/g at 30, 60, 120 min pi, respectively) with very fast blood clearance (1.09 ± 0.20%ID/g at 30 min pi and 0.38 ± 0.10%ID/g at 120 min pi). The kidney uptake of **8** was 17.47 ± 2.00%ID/g at 30 min pi and 8.01 ± 0.68% ID/g at 120 min pi. Its liver uptake was 3.28 ± 0.44%ID/g and 2.47 ± 0.25%ID/g at 30 and 120 min pi, respectively. The muscle uptake of **8** was 2.33 ± 0.61%ID/g at 30 min pi and 1.05 ± 0.42%ID/g at 120 min pi, The tumor/blood and tumor/liver ratios for **7** and **8** were almost identical within the experimental error, but the tumor/muscle ratios of **8** were better ($p < 0.05$) than those of **7** over the 2 h study period (Figure 3).

Blocking Experiment. The blocking experiment was used to demonstrate the integrin $\alpha_v\beta_3$ specificity. In this experiment,
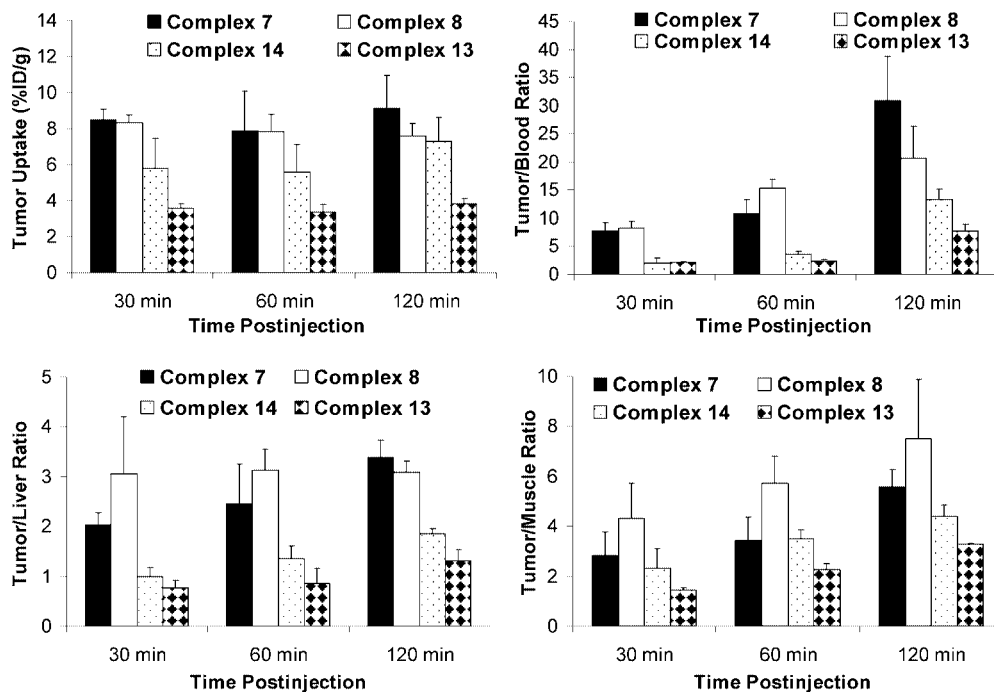
Figure 3. Comparison of tumor uptake and selected T/B ratios between **7**, **8**, **13**, and **14** in athymic nude mice ($n = 4$) bearing MDA-MB-435 human breast cancer xenografts.
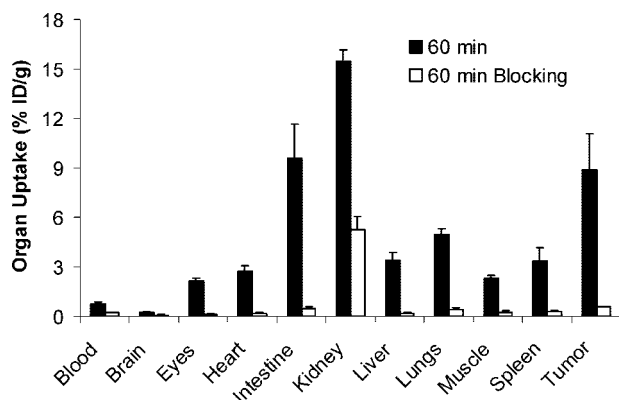

Figure 4. Comparison of organ uptake for **7** at 60 min pi in the absence/presence of excess **1**. Each data point represents an average of biodistribution data in four animals.

complex **7** was used as the radiotracer and **1** as the blocking agent at a dose of ~350 μg per mouse (or ~14 mg/kg). Figure 4 compares the selected organ uptake of **7** in the absence/presence of **1** at 60 min pi. Coinjection of **1** resulted almost complete blockage of the tumor uptake for **7** (0.55 ± 0.04%ID/g with **1** vs 8.86 ± 2.23%ID/g without **1**). There was also a significant reduction in radioactivity accumulation in noncancerous organs, such as the eyes, heart, intestine, kidneys, lungs, liver, muscle, and spleen.

Biodistribution Characteristics in Glioma Model. To further confirm our findings from the MDA-MB-435 breast cancer model, we also evaluated the biodistribution properties of **7** and **10** using athymic nude mice bearing U87MG glioma xenografts. The tumor size in these two tumor-bearing models was very close (0.1−0.5 g). Results from these studies will allow us to demonstrate the superiority of **7** over **10** and to compare the tumor uptake of **7** in two different tumor-bearing animal models. Figure 5 compares their tumor uptake and T/B ratios. Detailed biodistribution data for **7** and **10** are summarized in Tables SIII and SIV of the Supporting Information.

In general, the normal organ uptake of **7** in the glioma-bearing mice was identical to that in those obtained in the breast cancer model. The tumor uptake of **7** was 13.43 ± 0.98%ID/g, 11.02 ± 2.34%ID/g, and 7.74 ± 1.25%ID/g at 30, 60, and 120 min pi, respectively, which were more than twice of that for **10** (6.70 ± 1.59%ID/g, 5.62 ± 1.12%ID/g, and 3.03 ± 0.54%ID/g at 30, 60, and 120 min pi, respectively). As a result, **7** had the tumor/blood ratios (9.19 ± 1.79 at 30 min pi and 29.02 ± 4.68 at 120 min pi) and tumor/liver ratios (2.85 ± 0.29 at 30 min pi and 2.39 ± 0.50 at 120 min pi) that were significantly better ($p < 0.01$) than those of **10** (tumor/blood ratio = 4.42 ± 0.40 at 30 min pi and 13.08 ± 3.84 at 120 min pi, and tumor/liver ratio = 1.95 ± 0.62 at 30 min pi and 1.40 ± 0.16 at 120 min pi). The kidney uptake of **10** (10.88 ± 2.02%ID/g at 30 min pi and 3.75 ± 0.48% ID/g at 120 min pi, respectively) was lower than half of that for **7** (23.33 ± 2.78%ID/g at 30 min pi and 9.99 ± 0.61%ID/g at 120 min pi). The muscle uptake of **10** (1.89 ± 0.42%ID/g at 30 min pi and 0.64 ± 0.11%ID/g at 120 min pi) was also significantly lower than that of **7** (2.72 ± 0.33%ID/g at 30 min pi and 1.25 ± 0.10%ID/g at 120 min pi).

Effect of Tumor Size. During biodistribution studies, we noticed that there is often a large variation in tumor size even if the same number of U87MG glioma cells were used for the same animal. Smaller tumors (<0.5 g) tend to have higher radiotracer uptake than large tumors regardless of the identity of radiotracer. To clarify the relationship between the radiotracer tumor uptake and tumor size, we added extra glioma-bearing mice into the 120-min group for **7** and breast tumor-bearing mice for **8**. Figure 6 shows the relationship between the tumor size and tumor uptake of **7** and **8**. In the glioma model, there is a linear relationship between the tumor size (0.02−0.7 g; $n = 10$) and the %ID tumor uptake of **7** with $R^2 = 0.9207$ (Figure 6A). As tumor size increases, the %ID tumor uptake also increases. If the tumor uptake is expressed as %/ID/g (Figure 6B), it seems that **7** has a narrow window to achieve the optimal %ID/g tumor uptake. When the tumor size is in the range of 0.1−0.25 g, **7** has the tumor
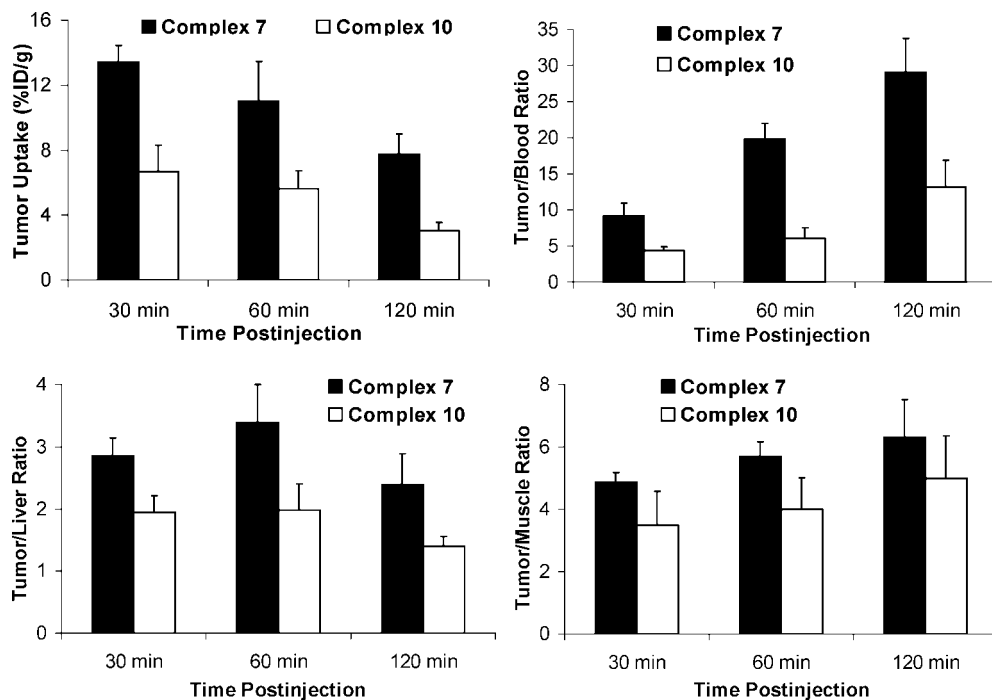
Figure 5. Direct comparison of tumor uptake and selected T/B ratios between **7** and **10** in the athymic nude mice ($n = 4$) bearing U87MG human glioma xenografts.
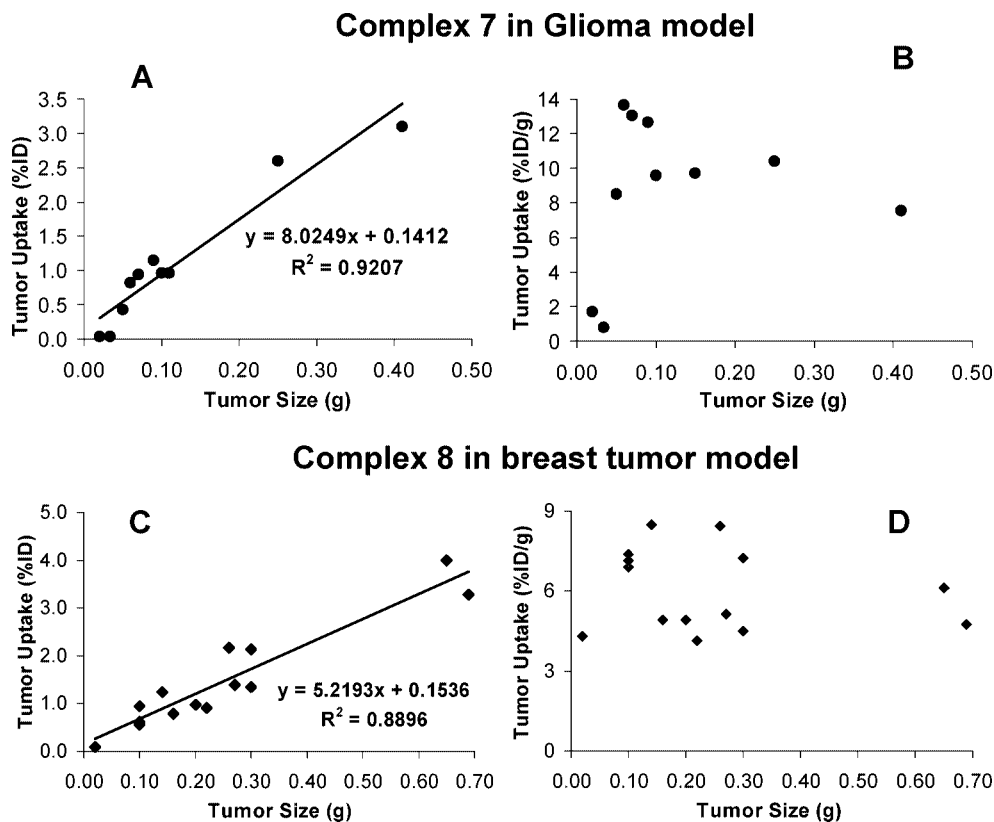
Complex 7 in Glioma model

Complex 8 in breast tumor model

Figure 6. The relationship between tumor size and tumor uptake expressed as %ID (left) and %ID/g (right) for **7** at 120 min pi in the athymic nude mice bearing the U87MG glioma xenografts ($n = 5$ and tumor number = 10), and for **8** at 120 min pi in the athymic nude mice bearing the MDA-MB-435 xenografts ($n = 7$ and tumor number = 14).

uptake between 8.0%ID/g and 14%ID/g. When the tumor size is too large (>0.4 g), its tumor uptake is <8.0%ID/g. When the tumor size is too small (<0.05 g), its tumor uptake is less than 2.0%ID/g. The linear relationship between tumor size ($0.03-0.7$ g; $n = 14$) and the radiotracer %ID tumor uptake was also observed for **8** with $R^2 = 0.8896$ (Figure 6C) in the breast cancer model. However, the distribution pattern of the %ID/g tumor uptake relative to the tumor size was more scattered for **8** as compared to that for **7** in the glioma model (Figure 6D). Apparently, the radiotracer tumor uptake (expressed as %ID and %ID/g) is dependent not only on the tumor size but also on the tumor type.

Complex 7 in Glioma model
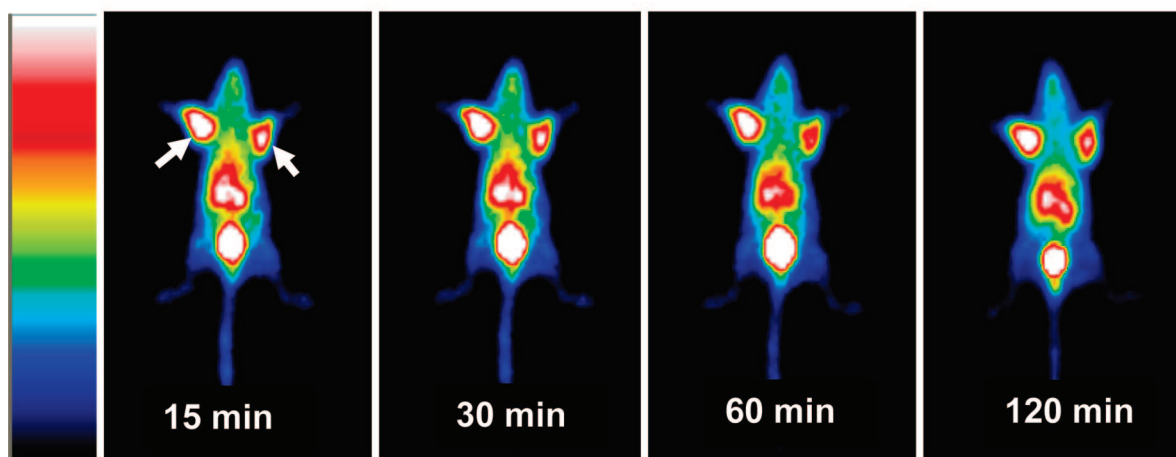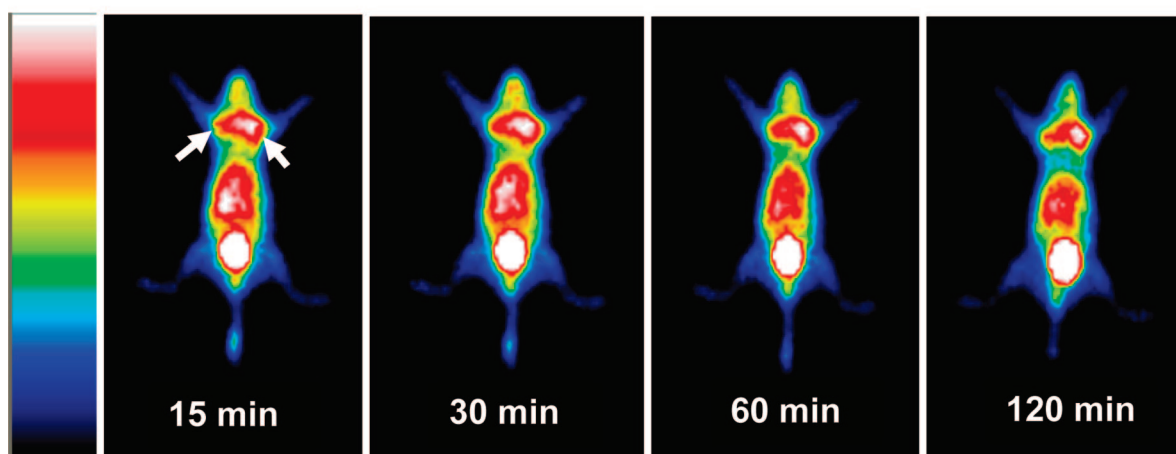

Complex 8 in breast tumor model

Figure 7. Top: static images of the tumor-bearing mice (U87MG glioma xenografts) administered with ∼1 mCi of **7** at 15, 30, 60, and 120 min pi. Bottom: static images of the tumor-bearing mice (MDA-MB435 breast cancer xenografts) administered with ∼1 mCi of **8** at 15, 30, 60, and 120 min pi. Arrows indicate the presence of tumors.

Metabolic Properties. We studied the metabolic stability of **7**, **8**, and **10** using normal athymic nude mice. Two animals were used for each ^{99m}Tc radiotracer. Figure SI of the Supporting Information shows typical radio-HPLC chromatograms of **7** in saline, in urine at 30 and 120 min pi, and in feces at 120 min pi. There were no metabolites detectable for **7** in the urine and feces samples over a 2 h study period. Similar metabolic stability was also observed for **8** (Figure SII, Supporting Information) and **10** (Figure SIII, Supporting Information).

Planar Imaging. Figure 7 shows static images of the athymic nude mice bearing U87MG glioma and MDA-MB435 breast cancer xenografts, respectively, at 15, 30, 60, and 120 min pi. All tumors were clearly visualized as early as 15 min pi with excellent contrast. No significant activity accumulation was detected in the liver and lungs. We also examined tumor detectability using **8** as the radiotracer. Figure 8 compares the 60 min static images of the tumor-bearing mice (U87MG glioma xenografts with tumor size in the range 0.10−0.80 g) administered with **8**. It was found that the tumors of ∼5 mm in diameter could be readily visualized as soon as **8** was injected.

Larger tumors (>0.45 g) had much better visualization than smaller ones (∼0.1 g).

Discussion

For a new integrin $\alpha_v\beta_3$-targeted radiotracer to be successful, it must show clinical indications for high-incidence tumor types, such as breast, prostate, colorectal, and lung cancers. The radiotracer should be able to have high tumor uptake with diagnostically useful T/B ratios in a short period of time (preferably <2 h pi). The radiotracer must be prepared in high yield and radiochemical purity with very high specific activity. In addition, it should be readily available at low cost for the radiotracer to assume a widespread clinical utility. Although PET imaging studies clearly show that the ^{18}F-labeled cyclic RGD monomers are able to localize the integrin $\alpha_v\beta_3$-positive tumors in cancer patients,[69−71] the relatively low tumor uptake, very high cost, and lack of preparative modules for the ^{18}F-labeled RGD peptides will severely limit their clinical utilities for noninvasive imaging of integrin $\alpha_v\beta_3$ expression in cancer patients. Therefore, there is a continuing need for the integrin $\alpha_v\beta_3$-targeted radiotracer that can be readily prepared in high
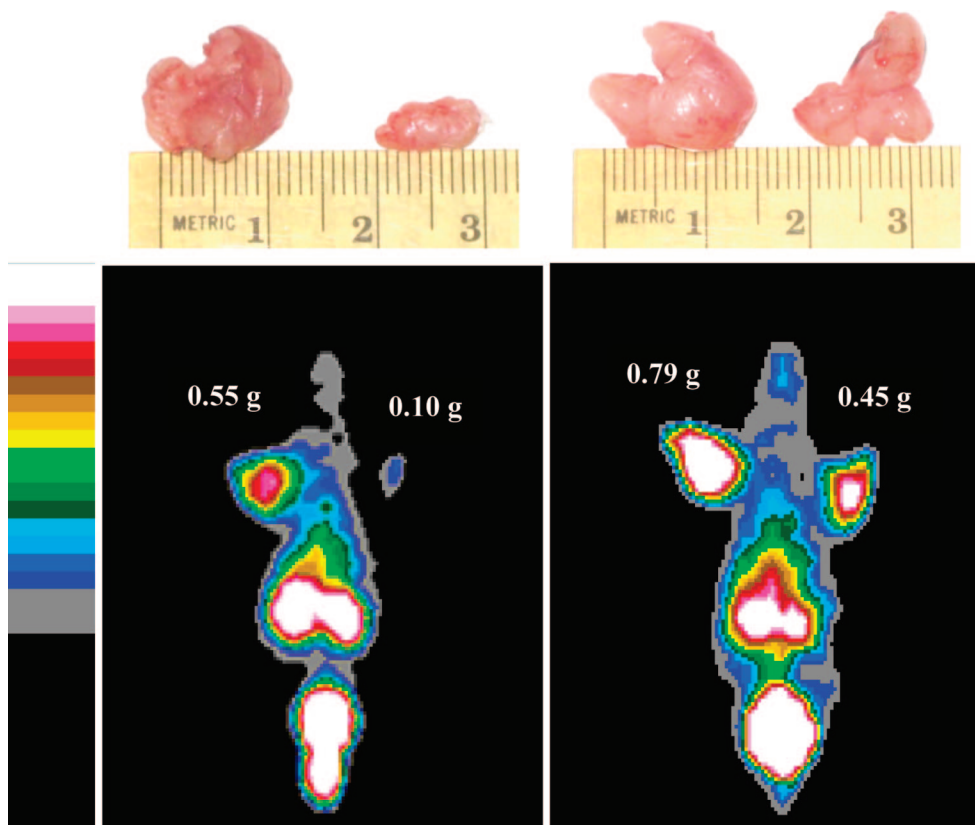
Figure 8. The 60 min static images of **8** in the athymic nude mice with different tumor sizes (0.10−0.80 g or 100−800 mm^3).

radiochemical purity with high specific activity. The ^{99m}Tc-labeled cyclic RGD peptide dimers described in this study satisfy this need due to the optimal nuclear properties, easy availability, and low cost of ^{99m}Tc,[72−74] the non-SnCl$_2$ formulation for routine clinical preparations of ^{99m}Tc-labeled cyclic RGD dimers, and their excellent biodistribution characteristics and excretion kinetics from noncancerous organs, particularly liver and kidneys.

In this study, we have successfully prepared two cyclic RGD dimer conjugates (**5** and **6**). Their ternary ligand ^{99m}Tc complexes **7** and **8** were prepared in high yield (RCP >95%) and with high specific activity (>10 Ci/μmol) using the non-SnCl$_2$ kit formulation. They were stable in the kit matrix for more than 6 h. In this respect, **7** and **8** offer significant advantages over the ^{18}F-labeled cyclic RGD peptide radiotracers, which often require several steps of radiosynthesis and tedious postlabeling chromatographic purification. Manual radiosynthesis and postlabeling chromatographic purification impose significant radiation exposure to radiopharmacists.

The integrin $\alpha_v\beta_3$ binding affinities against ^{125}I-echistatin follow the order of **12** (IC$_{50}$ = 7.2 ± 1.5 nM) ≫ **5** (IC$_{50}$ = 60.3 ± 4.4 nM) ∼ **6** (IC$_{50}$ = 61.1 ± 2.1 nM) > **11** (IC$_{50}$ = 112.2 ± 20.8 nM) ≫ **9** (IC$_{50}$ = 357.5 ± 8.3 nM). The addition of G$_3$ linkers between two cyclic RGD motifs is responsible for the improved integrin $\alpha_v\beta_3$ binding affinity of **5** and **6**. However, the addition of an extra G$_3$ linker between HYNIC and **3** had little impact on integrin $\alpha_v\beta_3$ binding affinity. It must be noted that the IC$_{50}$ value depends largely on the radioligand (^{125}I-echistatin vs ^{125}I-c(RGDyK)) and tumor cell lines (U87MG vs MDA-MB-435) used in the in vitro competition assay. Caution should be taken when comparing the IC$_{50}$ values of cyclic RGD peptides with those reported in the literature.

The distance between the two cyclic RGD motifs is 6 bonds in **11** and 26 bonds in **5** excluding side arms of K-residues.

The higher integrin $\alpha_v\beta_3$ binding affinity of **5** (IC$_{50}$ = 60.3 ± 4.4 nM) than that of **11** (IC$_{50}$ = 112.2 ± 20.8 nM) suggests that **5** is bivalent in binding to the integrin $\alpha_v\beta_3$ (Figure 1A), and the distance between two cyclic RGD motifs in **11** is probably too short for simultaneous integrin $\alpha_v\beta_3$ binding (Figure 1B). This conclusion is supported by the higher tumor uptake of **7** (8.48 ± 0.59%ID/g at 30 min pi and 9.11 ± 1.83%ID/g at 120 min pi) than that of **13** (3.49 ± 0.62%ID/g at 30 min pi and 3.82 ± 0.54%ID/g at 120 min pi) in the same animal model.[57,60] If they were bivalent in binding to integrin $\alpha_v\beta_3$, **5** and **11** would have had the same integrin $\alpha_v\beta_3$ binding affinity, whereas **7** and **13** would have had similar tumor uptake. Even though **11** is not bivalent, the binding of one RGD motif may significantly increase the local RGD concentration in the vicinity of neighboring integrin $\alpha_v\beta_3$ sites. This may explain why **11** (IC$_{50}$ = 112.2 ± 20.8 nM) has higher integrin $\alpha_v\beta_3$ affinity than **9** (IC$_{50}$ = 357.5 ± 8.3 nM) and the radiolabeled cyclic RGD dimers have better tumor uptake than their monomeric analogues.[50−54,56−68] Therefore, **3** and **4** are better targeting biomolecules than **1** for the future development of integrin $\alpha_v\beta_3$-targeted radiotracers.

In **12**, there are four identical cyclic RGD motifs. The longest distance between two adjacent RGD motifs is 16 bonds (excluding side arms of K-residues). The integrin $\alpha_v\beta_3$ binding affinity of **12** (IC$_{50}$ = 7.2 ± 1.5 nM) is much higher than those of **11** (IC$_{50}$ = 112.2 ± 20.8 nM) and **5** (IC$_{50}$ = 60.3 ± 4.4 nM). On the basis of these results, one *might* suggest that the higher tumor uptake of **14** (5.78 ± 0.67%ID/g at 30 min pi and 7.30 ± 1.32%ID/g at 120 min pi) than that of **9** (3.49 ± 0.62%ID/g at 30 min pi and 3.82 ± 0.54%ID/g at 120 min pi) is most likely caused by a combination of the simultaneous integrin $\alpha_v\beta_3$ binding of two adjacent RGD motifs and the presence of four cyclic RGD motifs in **12**.[60] The lower tumor uptake for **14** (5.78 ± 0.67%ID/g at 30 min pi and 7.30 ±

1.32%ID/g at 120 min pi) than that of **7** (8.48 ± 0.59%ID/g at 30 min pi and 9.11 ± 1.83%ID/g at 120 min pi) is probably caused by the tumor size difference during biodistribution studies.

Complex **7** has significant advantages over **14** with respect to radioactivity accumulation in noncancerous organs. For example, the liver uptake of **7** (2.68 ± 0.46%ID/g at 120 min pi) was lower ($p < 0.01$) than that of **14** (4.09 ± 0.59%ID/g at 120 min pi). Its tumor/liver ratios (2.85 ± 0.29 and 2.39 ± 0.50 at 30 and 120 min pi, respectively) are better ($p < 0.01$) than those for **14** (1.25 ± 0.27 and 1.78 ± 0.27 at 30 and 120 min pi, respectively). The tumor/muscle ratios of **7** (2.84 ± 0.93 at 30 min pi and 5.57 ± 0.69 at 120 min pi) are much better ($p < 0.01$) than those of **9** (1.44 ± 0.25 at 30 min pi and 3.28 ± 0.32%ID/g at 120 min pi),[32] and **14** (2.50 ± 0.70%ID/g at 30 min pi and 3.69 ± 0.96%ID/g at 120 min pi).[58] The kidney uptake of **7** (10.74 ± 2.43% ID/g at 120 min pi) is less than half of that of **10** (25.93 ± 2.52%ID/g at 120 min pi). The higher kidney uptake of **14** is most likely caused by the presence of four R-residues in **14** as compared to two R-residues in **5**. Thus, **3** and **4** are better targeting biomolecules than **2** for the future development of integrin $\alpha_v\beta_3$-targeted radiotracers.

Complex **8** has the tumor uptake (%ID/g), tumor/blood, and tumor/liver ratios comparable to those of **7** (Figure 3), but its tumor/muscle ratios are significantly better ($p < 0.01$) than those of **7** over the 2 h period. Because the tumor uptake of **7** is almost completely blocked by coinjection of excess **1** (Figure 4), we believe that its tumor uptake is integrin $\alpha_v\beta_3$-mediated. The uptake blockage in eyes, heart, intestine, kidneys, lungs, liver, and spleen suggests that the uptake of **7** in these organs is at least partially integrin $\alpha_v\beta_3$-mediated. This conclusion is supported by the immunohistopathological studies,[53,54] which showed a strong positive staining of endothelial cells of the small glomeruli vessels in kidneys and weak staining in the branches of the hepatic portal vein.

The glioma uptake of **7** (13.43 ± 0.98%ID/g at 30 min pi and 11.02 ± 2.34%ID/g at 60 min pi) is significantly higher ($p < 0.01$) than its breast tumor uptake (8.48 ± 0.59%ID/g at 30 min pi and 7.86 ± 2.23%ID/g at 60 min pi). This seems consistent with the fact that the U87MG glioma cells have a higher level of integrin $\alpha_v\beta_3$ expression than MDA-MB-435 breast tumor cells.[53,54] However, this difference disappears at 120 min pi (7.74 ± 1.25%ID/g in glioma-bearing mice and 9.11 ± 1.83%ID/g in breast tumor-bearing mice). At this moment, it is unclear why the uptake of **7** increases in the breast tumor while it decreases in the glioma.

Noninvasive imaging of molecular markers, such as integrin $\alpha_v\beta_3$, is highly desirable for patient selection before antiangiogenic treatment and for more effective monitoring of therapeutic efficacy in the integrin $\alpha_v\beta_3$-positive cancer patients. The %ID tumor uptake reflects the integrin $\alpha_v\beta_3$ expression level on both tumor cells and endothelial cells of the tumor neovasculature. The %ID/g tumor uptake reflects the integrin $\alpha_v\beta_3$ density. When the tumor is small (<0.05 g or 50 mm³), there is little angiogenesis with low blood flow and low integrin $\alpha_v\beta_3$ expression. As a result, the %ID and %ID/g tumor uptake values of **7** are low in the glioma model (Figure 6: A and B). When tumors are in their rapid growing stage ($0.1-0.5$ g or $100-500$ mm³), the microvessel and integrin $\alpha_v\beta_3$ density is high. Its %ID/g tumor uptake is high (Figure 6B). As tumors grow, the total integrin $\alpha_v\beta_3$ level is increased, and the %ID tumor uptake increases (Figure 6A). In contrast, the microvessel density decreases due to maturity of blood vessels, and so is the integrin $\alpha_v\beta_3$ density due to larger interstitial space.[78] In addition, parts

of the tumor may become necrotic, leading to lower integrin $\alpha_v\beta_3$ density in larger tumors. As a result, the %ID/g tumor uptake of **7** in larger tumors (>0.5 g or 500 mm³) is lower than that of smaller ones (Figure 6B). In the breast tumor model, there is also a linear relationship between the tumor size and %ID tumor uptake of **8** (Figure 6C). However, its %ID/g tumor uptake values are more scattered as the tumor size changes (Figure 6D). The radiotracer tumor uptake depends not only on the tumor size but also on the tumor type. The linear relationship between the tumor size and the radiotracer %ID tumor uptake suggests that both **7** and **8** are useful for noninvasive monitoring of the tumor integrin $\alpha_v\beta_3$ expression.

Tumors must have sufficient radioactivity counts to be detectable. In this study, we found that tumors of >5 mm in diameter could be visualized with excellent contrast as early as 15 min postinjection of **7** and **8** (Figure 7). The most visible organs at 120 min pi are tumors, kidneys, and bladder. Larger tumors have much better visualization than the smaller ones (Figure 8). The tumor detection limit is ~5 mm in diameter using a modified clinical SPECT camera. With the newer high resolution SPECT cameras or SPECT/CT, the tumor detection limit might be significantly lower using **7** and **8** as radiotracers. Both **7** and **8** are useful for early detection of integrin $\alpha_v\beta_3$-positive tumors.

Extensive metabolic degradation was observed for the ^{99m}Tc-labeled cyclic RGD monomer,[35] dimer,[57,58] tetramer,[60,61] and the ^{64}Cu-labeled RGD tetramer in kidneys and urine samples.[54] However, the metabolism study shows that both **7** and **8** remain intact during their excretion from renal and hepatobiliary routes. It is unclear why **7** and **8** have such a high metabolic stability during excretion from renal and hepatobiliary routes (Figures SI and SIII of the Supporting Information), while **13** and **14** undergo extensive metabolism during excretion from the hepatobiliary route.

Conclusion

In summary, we have successfully prepared two new cyclic RGD peptide conjugates, **5** and **6**, and evaluated complexes **7** and **8** as radiotracers for imaging integrin $\alpha_v\beta_3$ expression in athymic nude mice bearing U87MG glioma and MDA-MB-435 breast cancer xenografts. The results from this study clearly show that the G_3 linkers between two cyclic RGD motifs in cyclic RGD dimers are useful for enhancing their integrin $\alpha_v\beta_3$ binding affinity and for improving the tumor uptake and clearance kinetics of their corresponding ^{99m}Tc radiotracers from noncancerous organs. In addition, **8** is readily prepared in high yield (RCP > 95%) and high specific activity (>10 Ci/μmol). Complex **8** offers significant advantages over the ^{18}F-labeled RGD peptides with respect to cost, availability, and easiness of routine preparation. Therefore, **8** is a very attractive radiotracer for the early detection of integrin $\alpha_v\beta_3$-positive tumors, and may have potential applications for noninvasive monitoring of tumor growth or shrinkage during antiangiogenic treatment.

Supporting Information Available: Detailed biodistribution data and T/B ratios for ^{99m}Tc-labeled cyclic RGD peptides are listed.

Figures illustrate typical radio-HPLC chromatograms of **7**, **8**, and **10**, respectively, in saline before injection, in the urine at 30 min pi, in the urine at 120 min pi, and in the feces at 120 min pi. This material is available free of charge via the Internet at http://pubs.acs.org.

References

(1) Folkman, J. Angiogenesis in cancer, vascular, rheumatoid and other disease. *Nat. Med.* **1995**, *1*, 27–31.

(2) Folkman, J. Role of angiogenesis in tumor growth and metastasis. *Semin. Oncol.* **2002**, *29*, 15–18.

(3) Mousa, S. A. Mechanisms of angiogenesis in vascular disorders: potential therapeutic targets. *Drugs Future* **1998**, *23*, 51–60.

(4) Mousa, S. A. Integrins as novel drug discovery targets: potential therapeutic and diagnostic implications. *Emerging Ther. Targets* **2000**, *4*, 143–153.

(5) Carmeliet, P. Mechanism of angiogenesis and atheriogenesis. *Nat. Med.* **2000**, *6*, 389–395.

(6) Bögler, O.; Mikkelsen, T. Angiogenesis in glioma: molecular mechanisms and roadblocks to translation. *Cancer J.* **2003**, *9*, 205–213.

(7) Hwang, R.; Varner, J. V. The role of integrins in tumor angiogenesis. *Hematol. Oncol. Clin. North. Am.* **2004**, *18*, 991–1006.

(8) Jin, H.; Varner, J. Integrins: roles in cancer development and as treatment targets. *Br. J. Cancer* **2004**, *90*, 561–565.

(9) Kumar, C. C. Integrin $\alpha_v\beta_3$ as a therapeutic target for blocking tumor-induced angiogenesis. *Curr. Drug Targets* **2003**, *4*, 123–131.

(10) Brooks, P. C.; Clark, R. A. F.; Cheresh, D. A. Requirement of vascular integrin $\alpha_v\beta_3$ for angiogenesis. *Science* **1994**, *264*, 569–571.

(11) Friedlander, M.; Brooks, P. C.; Shaffer, R. W.; Kincaid, C. M.; Varner, J. A.; Cheresh, D. A. Definition of two angiogenic pathways by distinct α_v integrin. *Science* **1995**, *270*, 1500–1502.

(12) Horton, M. A. The $\alpha_v\beta_3$ integrin "vitronectin receptor". *Int. J. Biochem. Cell Biol.* **1997**, *29*, 721–725.

(13) Bello, L.; Francolini, M.; Marthyn, P.; Zhang, J. P.; Carroll, R. S.; Nikas, D. C.; Strasser, J. F.; Villani, R.; Cheresh, D. A.; Black, P. M. Alpha(v)beta3 and alpha(v)beta5 integrin expression in glioma periphery. *Neurosurgery* **2001**, *49*, 380–389.

(14) Meitar, D.; Crawford, S. E.; Rademaker, A. W.; Cohn, S. L. Tumor angiogenesis correlates with metastatic disease, N-*myc*-amplification, and poor outcome in human neuroblastoma. *J. Clin. Oncol.* **1996**, *14*, 405–414.

(15) Gasparini, G.; Brooks, P. C.; Biganzoli, E.; Vermeulen, P. B.; Bonoldi, E.; Dirix, L. Y.; Ranieri, G.; Miceli, R.; Cheresh, D. A. Vascular integrin $\alpha_v\beta_3$: a new prognostic indicator in breast cancer. *Clin. Cancer Res.* **1998**, *4*, 2625–2634.

(16) Albelda, S. M.; Mette, S. A.; Elder, D. E.; Stewart, R. M.; Damjanovich, L.; Herlyn, M.; Buck, C. A. Integrin distribution in maliganant melanoma: association of the beta3 subunit with tumor progression. *Cancer Res.* **1990**, *50*, 6757–6764.

(17) Falcioni, R.; Cimino, L.; Gentileschi, M. P.; D'Agnano, I.; Zupi, G.; Kennel, S. J.; Sacchi, A. Expression of beta 1, beta 3, beta 4, and beta 5 integrins by human lung carcinoma cells of different histotypes. *Exp. Cell Res.* **1994**, *210*, 113–122.

(18) Sengupta, S.; Chattopadhyay, N.; Mitra, A.; Ray, S.; Dasgupta, S.; Chatterjee, A. Role of $\alpha_v\beta_3$ integrin receptors in breast tumor. *J. Exp. Clin. Cancer Res.* **2001**, *20*, 585–590.

(19) Felding-Habermann, B.; Mueller, B. M.; Romerdahl, C. A.; Cheresh, D. A. Involvement of integrin alpha V gene expression in human melanoma tumorigenicity. *J. Clin. Invest.* **1992**, *89*, 2018–2022.

(20) Zitzmann, S.; Ehemann, V.; Schwab, M. Arginine-Glycine-Aspartic acid (RGD)-peptide binds to both tumor and tumor endothelial cells in vivo. *Cancer Res.* **2002**, *62*, 5139–5143.

(21) Weber, W. A.; Haubner, R.; Vabuliene, E.; Kuhnast, B.; Webster, H. J.; Schwaiger, M. Tumor angiogenesis targeting using imaging agents. *Q. J. Nucl. Med.* **2001**, *45*, 179–182.

(22) Costouros, N. G.; Diehn, F. E.; Libutti, S. K. Molecular imaging of tumor angiogenesis. *J. Cell. Biochem. Suppl.* **2002**, *39*, 72–78.

(23) Liu, S.; Edwards, D. S. Fundamentals of receptor-based diagnostic metalloradiopharmaceuticals. *Top. Curr. Chem.* **2002**, *222*, 259–278.

(24) Van de Wiele, C.; Oltenfreiter, R.; De Winter, O.; Signore, A.; Slegers, G.; Dieckx, R. A. Tumor angiogenesis pathways: related clinical issues and implications for nuclear medicine imaging. *Eur. J. Nucl. Med.* **2002**, *29*, 699–709.

(25) Liu, S.; Robinson, S. P.; Edwards, D. S. Integrin $\alpha_v\beta_3$ directed radiopharmaceuticals for tumor imaging. *Drugs Future* **2003**, *28*, 551–564.

(26) McDonald, D. M.; Choyke, P. Imaging Angiogenesis: from microscope to clinic. *Nat. Med.* **2003**, *9*, 713–725.

(27) Haubner, R.; Wester, H. R. Radiolabeled tracers for imaging of tumor angiogenesis and evaluation of anti-angiogenic therapies. *Curr. Pharm. Des.* **2004**, *10*, 1439–1455.

(28) Liu, S.; Robinson, S. P.; Edwards, D. S. Radiolabeled integrin $\alpha_v\beta_3$ antagonists as radiopharmaceuticals for tumor radiotherapy. *Top. Curr. Chem.* **2005**, *252*, 117–153.

(29) Chen, X. Multimodality imaging of tumor integrin $\alpha_v\beta_3$ expression. *Mini-Rev. Med. Chem.* **2006**, *6*, 227–234.

(30) D'Andrea, L. D.; Del Gatto, A.; Pedone, C.; Benedetti, E. Peptide-based molecules in angiogenesis. *Chem. Biol. Drug Des.* **2006**, *67*, 115–126.

(31) Meyer, A.; Auremheimer, J.; Modlinger, A.; Kessler, H. Targeting RGD recognizing integrins: drug development, biomaterial research, tumor imaging and targeting. *Curr. Pharm. Des.* **2006**, *12*, 2723–2747.

(32) Liu, S. Radiolabeled multimeric cyclic RGD peptides as integrin $\alpha_v\beta_3$-targeted radiotracers for tumor imaging. *Mol. Pharm.* **2006**, *3*, 472–487.

(33) Cai, W.; Chen, X. Multimodality imaging of tumor angiogenesis. *J. Nucl. Med.* **2008**, *49*, 113S–128S.

(34) Huabner, R.; Wester, H. J.; Senekowitsch-Schmidtke, R.; Diefenbach, B.; Kessler, H.; Stöcklin, G.; Schwaiger, M. RGD-peptides for tumor targeting: biological evaluation of radioiodinated analogs and introduction of a novel glycosylated peptide with improved biokinetics. *J. Labelled Compd. Radiopharm.* **1997**, *40*, 383–385.

(35) Haubner, R.; Bruchertseifer, F.; Bock, M.; Schwaiger, M.; Wester, H. J. Synthesis and biological evaluation of ^{99m}Tc-labeled cyclic RGD peptide for imaging integrin $\alpha_v\beta_3$ expression. *Nuklearmedizin* **2004**, *43*, 26–32.

(36) Haubner, R.; Wester, H. J.; Reuning, U.; Senekowisch-Schmidtke, R.; Diefenbach, B.; Kessler, H.; Stöcklin, G.; Schaiger, M. Radiolabeled $\alpha_v\beta_3$ integrin antagonists: a new class of tracers for tumor imaging. *J. Nucl. Med.* **1999**, *40*, 1061–1071.

(37) Sivolapenko, G. B.; Skarlos, D.; Pectasides, D.; Stathopoulou, E.; Milonakis, A.; Sirmalis, G.; Stuttle, A.; Courtenay-Luck, N. S.; Konstantinides, K.; Epenetos, A. A. Imaging of metastatic melanoma utilizing a technetium-99m labeled RGD-containing synthetic peptide. *Eur. J. Nucl. Med.* **1998**, *25*, 1383–1389.

(38) Haubner, R.; Wester, H. J.; Burkhart, F.; Senekowisch-Schmidtke, R.; Weber, W.; Goodman, S. L.; Kessler, H.; Schwaiger, M. Glycolated RGD-containing peptides: tracer for tumor targeting and angiogenesis imaging with improved biokinetics. *J. Nucl. Med.* **2001**, *42*, 326–336.

(39) Haubner, R.; Wester, H. J.; Weber, W. A.; Mang, C.; Ziegler, S. I.; Goodman, S. L.; Senekowisch-Schmidtke, R.; Kessler, H.; Schwaiger, M. Noninvasive imaging of $\alpha_v\beta_3$ integrin expression using 18F-labeled RGD-containing glycopeptide and positron emission tomography. *Cancer Res.* **2001**, *61*, 1781–1785.

(40) Thumshirn, G.; Hersel, U.; Goodman, S. L.; Kessler, H. Multimeric cyclic RGD peptides as potential tools for tumor targeting: solid-phase peptide synthesis and chemoselective oxime ligation. *Chem.—Eur. J.* **2003**, *9*, 2717–2725.

(41) Poethko, T.; Schottelius, M.; Thumshirn, G.; Herz, M.; Haubner, R.; Henriksen, G.; Kessler, H.; Schwaiger, M.; Wester, H. J. Chemoselective preconjugate radiohalogenation of unprotected mono- and multimeric peptides via oxime formation. *Radiochim. Acta* **2004**, *92*, 317–327.

(42) Poethko, T.; Schottelius, M.; Thumshirn, G.; Hersel, U.; Herz, M.; Henriksen, G.; Kessler, H.; Schwaiger, M.; Wester, H. J. Two-step methodology for high yield routine radiohalogenation of peptides: 18F-labeled RGD and octreotide analogs. *J. Nucl. Med.* **2004**, *45*, 892–902.

(43) Alves, S.; Correia, J. D. G.; Gano, L.; Rold, T. L.; Prasanphanich, A.; Haubner, R.; Rupprich, M.; Alberto, R.; Decristoforo, C.; Snatos, I.; Smith, C. J. In vitro and in vivo evaluation of a novel ^{99m}Tc(CO)3-pyrazolyl conjugate of cyclo-(Arg-Gly-Asp-D-Tyr-Lys). *Bioconjugate Chem.* **2007**, *18*, 530–537.

(44) Fani, M.; Psimadas, D.; Zikos, C.; Xanthopoulos, S.; Loudos, G. K.; Bouziotis, P.; Varvarigou, A. D. Comparative evaluation of linear and cyclic ^{99m}Tc-RGD peptides for targeting of integrins in tumor angiogenesis. *Anticancer Res.* **2006**, *26*, 431–434.

(45) Su, Z. F.; Liu, G.; Gupta, S.; Zhu, Z.; Rusckowski, M.; Hnatowich, D. J. In vitro and in vivo evaluation of a technetium-99m-labeled cyclic RGD peptide as specific marker of $\alpha_v\beta_3$ integrin for tumor imaging. *Bioconjugate Chem* **2002**, *13*, 561–570.

(46) Decristoforo, C.; Faintuch-Linkowski, B.; Rey, A.; vo Guggenberg, E.; Rupprich, M.; Hernandez-Gonzales, I.; Rodrigo, T.; Haubner, R. [^{99m}Tc]HYNIC-RGD for imaging integrin $\alpha_v\beta_3$ expression. *Nucl. Med. Biol.* **2006**, *33*, 945–952.

(47) Chen, X.; Park, R.; Tohme, M.; Shahinian, A. H.; Bading, J. R.; Conti, P. S. MicroPET and autoradiographic imaging of breast cancer α_v-integrin expression using ^{18}F- and ^{64}Cu-labeled RGD peptide. *Bioconjugate Chem.* **2004**, *15*, 41–49.

(48) Chen, X.; Park, R.; Shahinian, A. H.; Tohme, M.; Khankaldyyan, V.; Bozorgzadeh, M. H.; Bading, J. R.; Moats, R.; Laug, W. E.; Conti, P. S. ^{18}F-labeled RGD peptide: initial evaluation for imaging brain tumor Angiogenesis. *Nucl. Med. Biol.* **2004**, *31*, 179–189.

(49) Chen, X.; Park, R.; Shahinian, A. H.; Bading, J. R.; Conti, P. S. Pharmacokinetics and tumor retention of ^{125}I-labeled RGD peptide are improved by PEGylation. *Nucl. Med. Biol.* **2004**, *31*, 11–19.

(50) Chen, X.; Liu, S.; Hou, Y.; Tohme, M.; Park, R.; Bading, J. R.; Conti, P. S. MicroPET imaging of breast cancer α_v-integrin expression with ^{64}Cu-labeled dimeric RGD peptides. *Mol. Imaging Biol.* **2004**, *6*, 350–359.

(51) Chen, X.; Tohme, M.; Park, R.; Hou, Y.; Bading, J. R.; Conti, P. S. MicroPET imaging of breast cancer α_v-integrin expression with ^{18}F-labeled dimeric RGD peptide. *Mol. Imaging* **2004**, *3*, 96–104.

(52) Wu, Y.; Zhang, X.; Xiong, Z.; Cheng, Z.; Fisher, D. R.; Liu, S.; Gambhir, S. S.; Chen, X. MicroPET imaging of glioma integrin $\alpha_v\beta_3$ expression using ^{64}Cu-labeled tetrameric RGD peptide. *J. Nucl. Med.* **2005**, *46*, 1707–1718.

(53) Zhang, X.; Xiong, Z.; Wu, Y.; Cai, W.; Tseng, J. R.; Gambhir, S. S.; Chen, X. Quantitative PET imaging of tumor integrin $\alpha_v\beta_3$ expression with ^{18}F-FPRGD2. *J. Nucl. Med.* **2006**, *47*, 113–121.

(54) Wu, Z.; Li, Z.; Chen, K.; Cai, W.; He, L.; Chin, F. T.; Li, F.; Chen, X. Micro-PET of tumor integrin $\alpha_v\beta_3$ expression using ^{18}F-labeled PEGylated tetrameric RGD peptide (18F-FPRGD4). *J. Nucl. Med.* **2007**, *48*, 1536–1544.

(55) Zhang, X.; Chen, X. Preparation and characterization of [99m]Tc(CO)3-BPy-RGD complex as $\alpha_v\beta_3$ integrin receptor-targeted imaging agent. *Appl. Radiat. Isot.* **2007**, *65*, 70–78.

(56) Liu, S.; Edwards, D. S.; Ziegler, M. C.; Harris, A. R.; Hemingway, S. J.; Barrett, J. A. ^{99m}Tc-Labeling of a hydrazinonicotinamide-conjugated vitronectin receptor antagonist. *Bioconjugate Chem.* **2001**, *12*, 624–629.

(57) Liu, S.; Hsieh, W. Y.; Kim, Y. S.; Mohammed, S. I. Effect of coligands on biodistribution characteristics of ternary ligand ^{99m}Tc complexes of a HYNIC-conjugated cyclic RGDfK dimer. *Bioconjugate Chem.* **2005**, *16*, 1580–1588.

(58) Jia, B.; Shi, J.; Yang, Z.; Xu, B.; Liu, Z.; Zhao, H.; Liu, S.; Wang, F. ^{99m}Tc-labeled cyclic RGDfK dimer: initial evaluation for SPECT imaging of glioma integrin $\alpha_v\beta_3$ expression. *Bioconjugate Chem.* **2006**, *17*, 1069–1076.

(59) Liu, S.; He, Z.; Hsieh, W. Y.; Kim, Y. S.; Jiang, Y. Impact of PKM linkers on biodistribution characteristics of the ^{99m}Tc-labeled cyclic RGDfK dimer. *Bioconjugate Chem.* **2006**, *17*, 1499–1507.

(60) Liu, S.; Hsieh, W. Y.; Jiang, Y.; Kim, Y. S.; Sreerama, S. G.; Chen, X.; Jia, B.; Wang, F. Evaluation of a ^{99m}Tc-labeled cyclic RGD tetramer for non-invasive imaging integrin $\alpha_v\beta_3$-positive breast cancer. *Bioconjugate Chem.* **2007**, *18*, 438–446.

(61) Liu, S.; Kim, Y. S.; Hsieh, W. Y.; Sreerama, S. G. Coligand effects on solution stability, biodistribution and metabolism of ^{99m}Tc-labeled cyclic RGDfK tetramer. *Nucl. Med. Biol.* **2008**, *35*, 111–121.

(62) Jia, B.; Liu, Z.; Shi, J.; Yu, Z.; Yang, Z.; Zhao, H.; He, Z.; Liu, S.; Wang, F. Linker effects on biological properties of ^{111}In-labeled DTPA conjugates of a cyclic RGDfK dimer. *Bioconjugate Chem.* **2008**, *19*, 201–210.

(63) Wang, J. J.; Kim, Y. S.; He, Z.; Liu, S. ^{99m}Tc-labeling of HYNIC-conjugated cyclic RGDfK dimer and tetramer using EDDA as coligand. *Bioconjugate Chem.* **2008**, *19*, 634–642.

(64) Janssen, M. L.; Oyen, W. J. G.; Dijkgraaf, I.; Massuger, L. F.; Frielink, C.; Edwards, D. S.; Rajopadhye, M.; Boonstra, H.; Corstens, F. H.; Boerman, O. C. Tumor targeting with radiolabeled $\alpha_v\beta_3$ integrin

binding peptides in a nude mouse model. *Cancer Res.* **2002**, *62*, 6146–6151.

(65) Janssen, M.; Oyen, W. J. G.; Massuger, L. F. A. G.; Frielink, C.; Dijkgraaf, I.; Edwards, D. S.; Rajopadyhe, M.; Corsten, F. H. M.; Boerman, O. C. Comparison of a monomeric and dimeric radiolabeled RGD-peptide for tumor targeting. *Cancer Biother. Radiopharm.* **2002**, *17*, 641–646.

(66) Dijkgraaf, I.; John, A. W.; Kruijtzer, J. A. W.; Liu, S.; Soede, A.; Oyen, W. J. G.; Corstens, F. H. M.; Liskamp, R. M. J.; Boerman, O. C. Improved targeting of the $\alpha_v\beta_3$ integrin by multimerization of RGD peptides. *Eur. J. Nucl. Med. Mol. Imaging* **2007**, *34*, 267–273.

(67) Dijkgraaf, I.; Liu, S.; Kruijtzer, J. A. W.; Soede, A. C.; Oyen, W. J. G.; Liskamp, R. M. J.; Corstens, F. H. M.; Boerman, O. C. Effect of linker variation on the in vitro and in vivo characteristics of an ^{111}In-labeled RGD Peptide. *Nucl. Med. Biol.* **2007**, *34*, 29–35.

(68) Line, B. R.; Mitra, A.; Nan, A.; Ghandehari, H. Targeting tumor angiogenesis: comparison of peptide and polymer−peptide conjugates. *J. Nucl. Med.* **2005**, *46*, 1552–1560.

(69) Kenny, L. M.; Coombes, R. C.; Oulie, I.; Contractor, K. B.; Miller, M.; Spinks, T. J.; McParland, B.; Cohen, P. S.; Hui, A.; Palmieri, C.; Osman, S.; Glaser, M.; Turton, D.; Al-Nahhas, A.; Anoagye, E. O. Phase I trial of the positron-emitting Arg-Gly-Asp (RGD) peptide radioligand ^{18}F-AH111585 in breast cancer patients. *J. Nucl. Med.* **2008**, *49*, 879–886.

(70) Beer, A. J.; Haubner, R.; Goebel, M.; Luderschmidt, S.; Spilker, M. E.; Webster, H. J.; Weber, W. A.; Schwaiger, M. Biodistribution and pharmacokineticss of the $\alpha_v\beta_3$-selective tracer ^{18}F-Galacto-RGD in cancer patients. *J. Nucl. Med.* **2005**, *46*, 1333–1341.

(71) Haubner, R.; Weber, W. A.; Beer, A. J.; Vabulience, E.; Reim, D.; Sarbia, M.; Becker, K. F.; Goebel, M.; Hein, R.; Wester, H. J.; Kessler, H.; Schwaiger, M. Noninvasive visuallization of the activated $\alpha_v\beta_3$ integrin in cancer patients by positron emission tomography and [^{18}F]Galacto-RGD. *PLOS Med.* **2005**, *2*, 244–252.

(72) Liu, S.; Edwards, D. S.; Barrett, J. A. ^{99m}Tc-labeling of highly potent small peptides. *Bioconjugate Chem.* **1997**, *8*, 621–636.

(73) Liu, S.; Edwards, D. S. ^{99m}Tc-labeled small peptides as diagnostic radiopharmaceuticals. *Chem. Rev.* **1999**, *99*, 2235–2268.

(74) Liu, S. 6-Hydrazinonicotinamide derivatives as bifunctional coupling agents for ^{99m}Tc-labeling of small biomolecules. *Top. Curr. Chem.* **2005**, *252*, 117–153.

(75) Harris, T. D.; Sworin, M.; Williams, N.; Rajopadhye, M.; Damphousse, P. R.; Glowacka, D.; Poirier, M. J.; Yu, K. Synthesis of stable hydrazones of a hydrazinonicotinyl-modified peptide for the preparation of ^{99m}Tc-labeled radiopharmaceuticals. *Bioconjugate Chem.* **1999**, *10*, 808–814.

(76) Liu, S.; Edwards, D. S.; Harris, A. R.; Ziegler, M. C.; Poirier, M. J.; Ewels, B. A.; DiLuzio, W. R.; Hui, P. Towards developing a non-SnCl2 formulation for RP444: a new radiopharmaceutical for thrombus imaging. *J. Pharm. Sci.* **2001**, *90*, 114–123.

(77) Liu, S.; Edwards, D. S.; Harris, A. R.; Heminway, S. J.; Barrett, J. A. Technetium complexes of a hydrazinonicotinamide-conjugated cyclic peptide and 2-hydrazinopyridine: Synthesis and characterization. *Inorg. Chem.* **1999**, *38*, 1326–1335.

(78) Jain, R. K. Transport of molecules in the tumor interstitium: a review. *Cancer Res.* **1987**, *47*, 3039–3051.